Biomacromolecules

Article

pubs.acs.org/Biomac

Influence of Magnetic Field Alignment of Cellulose Whiskers on the Mechanics of All-Cellulose Nanocomposites

Tanittha Pullawan, Arthur N. Wilkinson, and Stephen J. Eichhorn*,†

Materials Science Centre, School of Materials, University of Manchester, Grosvenor Street, Manchester, M13 9PL, United Kingdom

Supporting Information

ABSTRACT: Orientation of cellulose nanowhiskers (CNWs) derived from tunicates, in an all-cellulose nanocomposite, is achieved through the application of a magnetic field. CNWs are incorporated into a dissolved cellulose matrix system and during solvent casting of the nanocomposite a magnetic field is applied to induce their alignment. Unoriented CNW samples, without the presence of a magnetic field, are also produced. The CNWs are found to orient under the action of the magnetic field, leading to enhanced stiffness and strength of the composites, but not to the level that is theoretically predicted for a fully aligned system. Lowering the volume fraction of the CNWs is shown to allow them to orient more readily in the magnetic field, leading to larger relative increases in the mechanical properties. It is shown, using polarized light microscopy, that the all-cellulose composites have a domain structure, with some domains showing pronounced orientation of CNWs and others where no preferred orientation occurs. Raman spectroscopy is used to both follow the position of bands located at ~1095 and ~895 cm^{-1} with deformation and also their intensity as a function rotation angle of the specimens. It is shown that these approaches give valuable independent information on the respective molecular deformation and orientation of the CNWs, and the molecules in the matrix phase, in oriented and nonoriented domains of all-cellulose composites. These data are then related to an increase in the level of molecular deformation in the axial direction, as revealed by the Raman technique. Little orientation of the matrix phase is observed under the action of the magnetic field indicating the dominance of the stiff CNWs in governing mechanical properties.

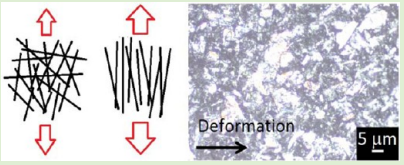

INTRODUCTION

Cellulose nanofibers have recently attracted a lot of attention due to their potential for making nanocomposite materials that display high stiffness and strengths.[1−5] This can be achieved with low weight penalties, and other properties such as transparency and low coefficients of thermal expansion.[1−5] These nanofibers come in a variety of forms, but most relevant to this work are those derived from plant and animal (tunicates) sources via acid hydrolysis; namely cellulose nanowhiskers (CNWs) or nanocrystals.[2,4] These rod-like CNWs can display high aspect ratios, and exhibit self-assembling chiral nematic behavior in suspension.[6] Directed orientation of a range of different forms of cellulose nanofibers during processing, through pressing and casting,[7] electrospinning,[8] conventional wet spinning,[9] application of magnetic[10−12] and electric fields,[13−15] and, most recently, by retaining a liquid crystalline nematic orientation in a composite microstructure[16] have been reported.

Orientation of CNWs using magnetic fields has been previously reported.[10−12] The physical reason for their orientation is that that the CNWs possess an anisotropic diagmetic susceptibility. CNWs possess a helical axis, perpendicular to the axis of their rod-like morphology. This helical axis has a greater diamagnetic susceptibility than the axial susceptibility, and so the axes of the CNWs align in a direction perpendicular to the magnetic field direction.[10−12]

The crystalline regions of cellulose intrinsically have a high stiffness; values in the range 100−150 GPa have been reported using modeling and experimental approaches.[17−21] There is a need to orient highly crystalline cellulose nanofibers in composite materials if this stiffness is to be fully utilized.

All-cellulose composites offer a route for making useful monocomponent reinforced materials that can exhibit transparency coupled with high mechanical properties.[22] The term "all-cellulose composite" was first used by Nishino et al.[23] and refers to a composite material where both the matrix and the fibrous reinforcement comprise cellulose. A number of studies have been published on the properties of all-cellulose composites, combining plant fibers with dissolved cellulose[24] or by selectively dissolving the surface of compacted cellulose networks to form the matrix.[25−28] In addition, precipitation of all-cellulose composites by partial dissolution of microcrystalline cellulose has also been reported;[29] all-cellulose nanocomposites have also been produced using a similar method.[30]

Understanding the interfaces in these so-called "interfaceless" composite materials[22] is critical, however, if we are to exploit their properties. Little work has been published on this subject. One paper showed how synchrotron X-ray diffraction could be used to follow the deformation in the matrix and reinforcing phases of an all-cellulose composite.[31] Similarly, Raman spectroscopy has been reported as a useful tool for following the deformation of the matrix and reinforcing phase

Received: May 14, 2012
Revised: June 26, 2012
Published: June 27, 2012

independently of each other.[32] The approach using Raman spectroscopy is to follow the shift in a characteristic peak in the spectrum relating to the main chain deformation of the polymer. Shifts in cellulose polymer fibers were first recorded by Hamad and Eichhorn[33] in 1997 and then subsequently in a large number of other cellulose fibers[34−37] and cellulose fiber-based composites.[38−41] In all-cellulose composites, of all the many vibrations that occur, the positions of two peaks located at ∼1095 and ∼895 cm^{-1} relating to the reinforcing phase (CNWs) and matrix material have been monitored during deformation giving unique insight into the coupling between these components.[32] The technique has also been reported to be useful for following the orientation of CNWs in a composite material during deformation, both in the wet and dry states.[42] This approach relies on the measurement of the intensity of a vibration that relates to the main chain of the polymer as a function of rotation of the specimen. Orientation of cellulose molecules coincident with the polarization direction of the laser exciting the vibration leads to a maximum intensity. If no preferred orientation is present, then the intensity remains invariant with rotation angle but changes dramatically for a pronounced orientation of molecular chains, that is, for oriented CNWs or fibrils within fibers.[7,42,43]

The present work combines both of these analytical approaches to give unique insight into the interfaces between the matrix phase and the CNWs in all-cellulose nanocomposites. CNWs are oriented, in a magnetic field, while the samples are cured. Interestingly the all-cellulose composites produced here have a domain structure, comprising oriented and nonoriented CNWs. These domains are interrogated using the Raman spectroscopic method. Comparisons are made with completely unoriented materials. Orientation of nanowhiskers and, additionally, the matrix phase of the nanocomposites is followed. This shows for the first time how the properties of these materials may be altered using magnetic field alignment to significantly alter stress-transfer processes.

EXPERIMENTAL SECTION

Materials. Tunicate CNWs were prepared by acid hydrolysis of tunicates (*Styela clava*) using sulphuric acid. After gutting, the tunicates were treated by heating in 3% w/w aqueous potassium hydroxide at 80 °C for 24 h to remove the outer walls of the tunicates, followed by mechanical agitation and scrubbing.[44] This step requires two more treatments with aqueous potassium hydroxide; this is a slight modification of the procedure, as previously reported by Yuan et al.[45] After neutralizing tunicates with 3 L of water, 5 mL acetic acid and 10 mL sodium hypochlorite solution (>4% chlorine) were added and heated up to 60 °C. After 1 h, 5 mL acetic acid and 10 mL sodium hypochlorite solution (>4% chlorine) were added until the tunicate's color changed to pure white. This bleaching procedure required two or three iterations, depending on the particular batch of tunicates. The bleached deproteinized walls were then washed with deionized water and disintegrated using a Warring blender, resulting in a fine cellulose pulp. Sulfate-functionalized CNWs were prepared by sulphuric acid hydrolysis of tunicates as described by Elazzouzi et al.[46] with minor modifications. Tunicate cellulose pulp was added to 48% sulphuric acid under vigorous mechanical stirring. The suspension was heated at 55 °C for 13 h while continually stirring. Then the dispersion was cooled, filtered, and washed with deionized water until neutrality was obtained. Finally, the CNWs were redispersed in 1 L of deionized water by overnight sonication and were then freeze-dried.

Characterization of the CNWs. To study the dispersibility of CNWs in both water and DMF (dimethylformamide), polarization filters were used to observe their flow birefringence. Suspensions of CNWs were sonicated for 6−8 h at room temperature. These suspensions were then transferred to a 5 mL glass vial and placed between two polarization filters, one rotated 90° relative to the other, to extinguish the light. If no flow birefringence pattern was observed, then the solutions were further sonicated.

Atomic force microscopy (AFM) was carried out to measure the dimensions of the CNWs. The samples were prepared by spin coating (model WS 650SZ spin coater, Laurell Technologies Corporation) the CNWs on a silicon wafer. Silicon wafers were cut into 1.0 × 1.0 cm^2 pieces and cleaned using Piranha solution (3:1 sulphuric acid to hydrogen peroxide; both chemicals from Sigma Aldrich) for 30 min. A 0.2 wt % cellulose whiskers suspension was dropped onto a cleaned silicon wafer and the spin coating was performed using a speed of 4000 rpm and an acceleration of 2100 rpm s^{-1} for 30 s.

AFM imaging was used with a Digital Instruments CP-II, Veeco Instruments Ltd., system at room temperature. The measurements of CNW dimensions were obtained in tapping mode, with a scan rate of 0.5 line s^{-1}. Images were processed using version 2.1.15 of the image processing and data analysis software. Heights of the CNWs were used to determine their widths due to a well-known tip broadening effect.

Preparation of Nanocomposite Specimens. All-cellulose nanocomposite films were prepared in three steps. The first step involved the activation of microcrystalline cellulose (Avicel, PH-101, Aldrich, particle size ∼ 50 μm) for 5 h in deionized water at room temperature to help swell the cellulose in preparation for dissolution. The activated cellulose was then dehydrated in acetone and *N*,*N*-dimethyl acetamide (DMAc; Sigma Aldrich) for 5 and 4 h, respectively. After that, DMAc was decanted from the dehydrated cellulose. A total of 8 g of LiCl was dispersed in 100 g of DMAc and then stirred at 120 °C for 30 min until the LiCl was completely dissolved. In the second step, the activated microcrystalline cellulose (2 g) was dissolved in 8% solution (by total weight) of LiCl/DMAc. The solution was then stirred using a magnetic stirrer at room temperature for 5−10 min and was stored in a sealed bottle for 1 week to allow further dissolution. Then the cellulose solution was centrifuged at 6000 rpm for 5 min to remove air bubbles and coagulate large cellulose particles. Finally, the CNW reinforced composite films were prepared by using a 15 v/v % concentration of nanowhiskers. CNWs were added to the matrix solution and ultrasonicated for 6 h to achieve good dispersions. The composite solutions were cast into a Petri dish and left under ambient conditions until a transparent gel had formed (2−3 h). Then the film was washed in deionized water to remove residual solvent and dried at ambient temperature.

Unidirectional reinforced nanocomposite films were produced from CNWs and cellulose solutions under an externally applied magnetic field. The magnetic alignment is driven by the characteristic negative diamagnetic anisotropy of the CNWs. Electron magnetic resonance (EMR) was used in order to align CNWs in a cellulose solution using a 1.2 T magnetic field. After adding CNWs in the matrix of dissolved cellulose, the composite suspension was then sonicated and cast on a glass slide. The glass slide was then placed in between the magnets of an electron paramagnetic resonance (EPR) machine (Manchester Interdisciplinary Biocenter, The University of Manchester) for 3 h. The nanocomposites were solvent cast while in the magnetic field, of field strength 1.2 T, until a transparent and dry film of an all-cellulose composite was obtained. The samples were then washed in distilled water for 1 h and placed back in the magnetic field for 3 h.

Mechanical Properties of Nanocomposite Specimens. All-cellulose composite films were cut into strips with a gauge length of 50 mm and width of 5 mm. The thicknesses of the composite samples were determined using a micrometer. Before testing, all specimens were equilibrated at a temperature of 23 ± 1 °C and 50 ± 5% relative humidity for 24 h; they had moisture contents of 5.2 ± 1.5% and 6.0 ± 2.5% for the 5 and 15 v/v % samples, respectively, measured as a percentage of their dried weight. These samples were tested using an Instron 1121 universal testing machine with Series IX software, and deformed in tension at a cross-head displacement rate of 1 mm min^{-1} and a 500 N (full scale) load cell was used to record the load. At least 10 samples were tested until failure at each gauge length. Load was converted to stress by dividing by the cross-sectional area of the

samples (assuming that this remains constant during deformation). The cross-sectional area of the samples was determined by multiplying the film thicknesses by their widths. Strain was assumed to be equal to the change in cross-head displacement divided by the original length of the samples, although it is acknowledged that local strain may differ from this. Young's moduli of the composite films were determined by calculating the initial slope of the stress−strain curves obtained by fitting a linear line to the initial data points (up to 0.5% strain).

Polarized Light Microscopy of Nanocomposite Specimens. An Olympus BH-2 optical microscope with 5× objective lens was used to observe anisotropic domains in the cellulose composite samples with the assistance of two polarized light filters. Samples were viewed under white light conditions.

Raman Spectroscopy of Nanocomposite Specimens. A Renishaw 1000 Raman imaging microscope and a 25 mW near-IR laser (785 nm) was used to record spectra from all-cellulose nanocomposite samples. The laser beam was attenuated to a lower power (~1 mW) and focused using a 50× objective lens to give a spot diameter of ~2 μm on the surface of the samples. The micromechanics of all-cellulose nanocomposites were investigated by deforming the samples incrementally using a Deben microtest tensile tester. All-cellulose nanocomposites were mounted and secured using Araldite epoxy resin onto paper cards, and the card was then fixed on a moveable block. The load applied to the sample was recorded by a load cell contained within the tensile tester. At each deformation increment a Raman spectrum was recorded using an exposure time of 40 s with four accumulations. Samples were deformed using strain increments of 0.1%. At each strain increment the stress was allowed to relax for a period (until stable) before a spectrum was recorded. Renishaw WIRE software was used to fit the obtained Raman spectra to determine the accurate central position of peaks at each deformation level. For this study, a mixed Gaussian−Lorentzian function was used to fit the Raman peaks to find their position using an algorithm based on the work of Marquardt.[47]

RESULTS AND DISCUSSION

Characterization of the CNWs. Polarized light images of suspensions of the CNWs, in both water and DMF are shown in Figure 1a. Both images show that the CNWs display flow birefringence, which indicates their excellent dispersion in solvents. A typical AFM image of the CNWs is shown in Figure 1b. It is clear that the CNWs have a rod-like nature, typical of this form of cellulose nanofiber. From a series of these images we obtained an aspect ratio of the CNWs of 72.8 ± 40.8. This figure is typical for tunicate-derived CNWs.[40,46] Given the large standard deviation on this value there is however clearly a large heterogeneity to the aspect ratio of the CNWs.

Mechanical Properties of Nanocomposite Specimens. Typical stress−strain curves for the all-cellulose nanocomposite samples are shown in Figure 2. All curves indicate characteristic nonlinear stress−strain behavior, typical for a regenerated cellulose film, as has been previously reported for other nanocomposite films made using this approach.[48,49] Mechanical properties data for these samples are reported in Supporting Information (Tables S1 and S2). The mechanical properties of a film of pure matrix material are similar to values obtained by Duchemin et al.[29] The pure matrix films obtained in the present study have lower mechanical properties than those previously reported by Gindl and Keckes.[30] They reported a tensile strength of 218 MPa and Young's modulus of 12 GPa for samples made from 2 wt % activated MCC in LiCl/DMAc. Duchemin et al.[29] suggested that low mechanical properties of all-cellulose nanocomposites could be due to factors such as precipitating the cellulose for different times and at different temperatures and humidities. Differences in the degree of

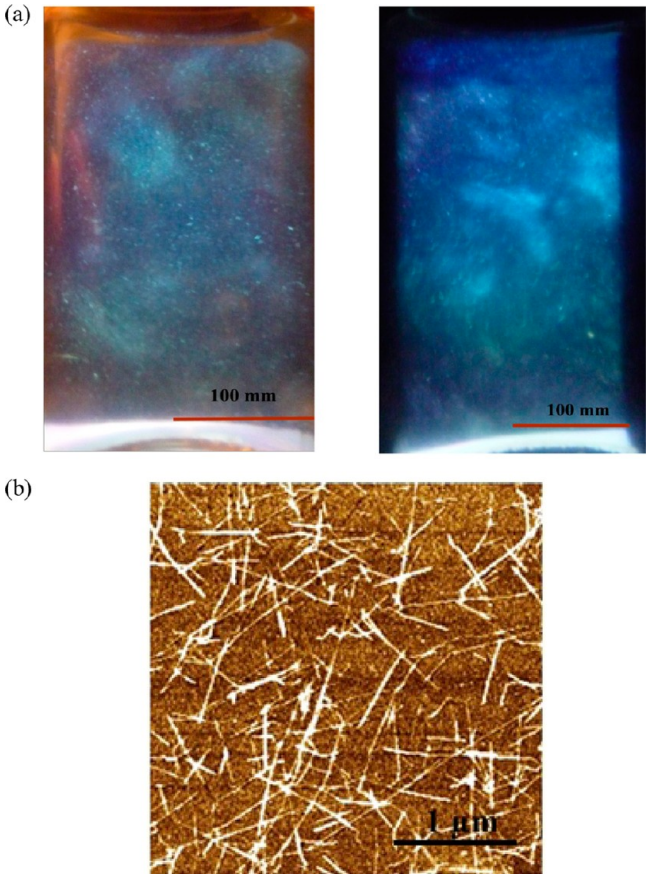

Figure 1. (a) Polarized light images of CNWs dispersed in water (left) and redispersed in DMF (right) prior to composite production; (b) An AFM image of CNWs.

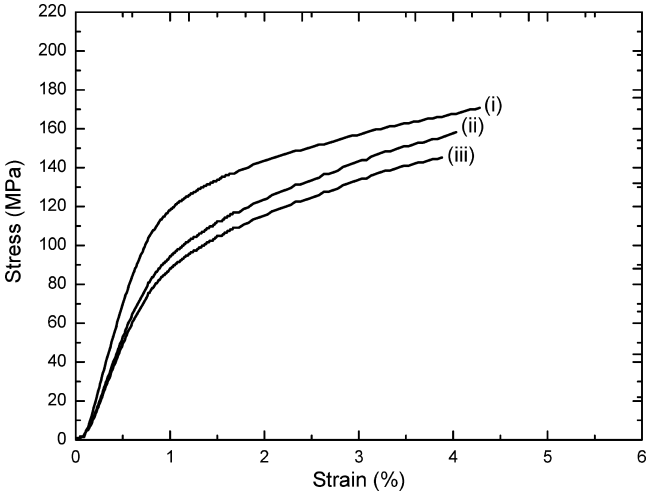

Figure 2. Typical stress−strain curves for all-cellulose nanocomposites (15 v/v %) produced both with and without the presence of a magnetic field; sample produced (i) within the magnetic field and deformed perpendicular to the field direction, (ii) without the presence of a magnetic field, and (iii) within the magnetic field and deformed parallel to the field direction.

polymerization of the cellulose source are also thought to govern eventual mechanical properties.[29,30,50]

Production of the all-cellulose nanocomposites within the magnetic field is thought to align the CNWs, resulting in significantly higher mechanical properties of samples deformed

dx.doi.org/10.1021/bm300746r | Biomacromolecules 2012, 13, 2528−2536

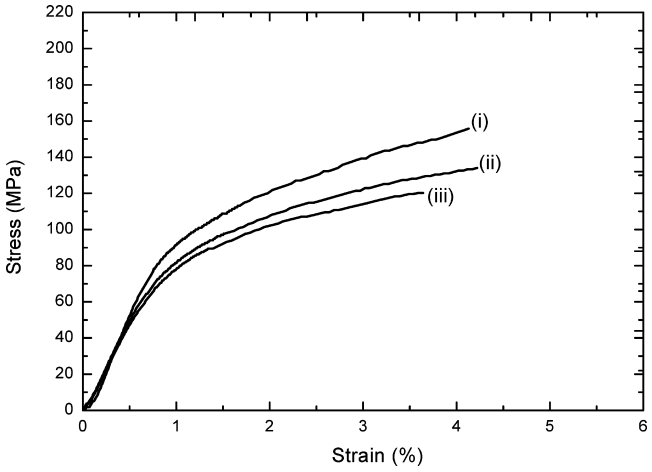

Figure 3. Typical stress−strain curves for all-cellulose nanocomposites (5 v/v %) produced both with and without the presence of a magnetic field; sample produced (i) within magnetic field and deformed perpendicular to field direction, (ii) without the presence of a magnetic field, and (iii) within magnetic field and deformed parallel to field direction.

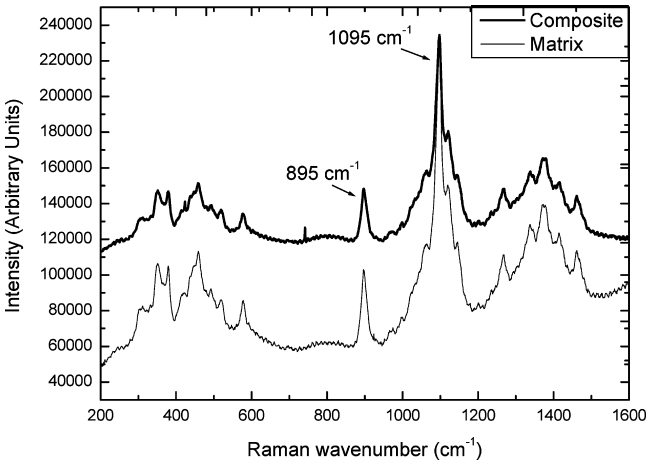

Figure 5. Typical Raman spectra obtained from an all-cellulose nanocomposite (containing 15 v/v % of CNWs) and matrix material. The positions of the bands located at ∼1095 and ∼895 cm^{-1} are indicated.

perpendicular to the magnetic field direction, that is, along the direction of the main axes of the aligned CNWs. Samples produced outside the magnetic field have mechanical properties significantly lower than those produced within the field. Finally, samples deformed parallel to the magnetic field direction exhibit the lowest mechanical properties of all. This is thought to be due to the fact that the CNWs have much lower transverse stiffness compared to along their axes, a result which has been recently confirmed by mechanical measurements using AFM.[51] As a control, to test this hypothesis, samples (i) and (iii) were cut in the opposite directions to see if equivalent mechanical data could be obtained. Data for these samples are also shown in Supporting Information (Table S1). It is clear

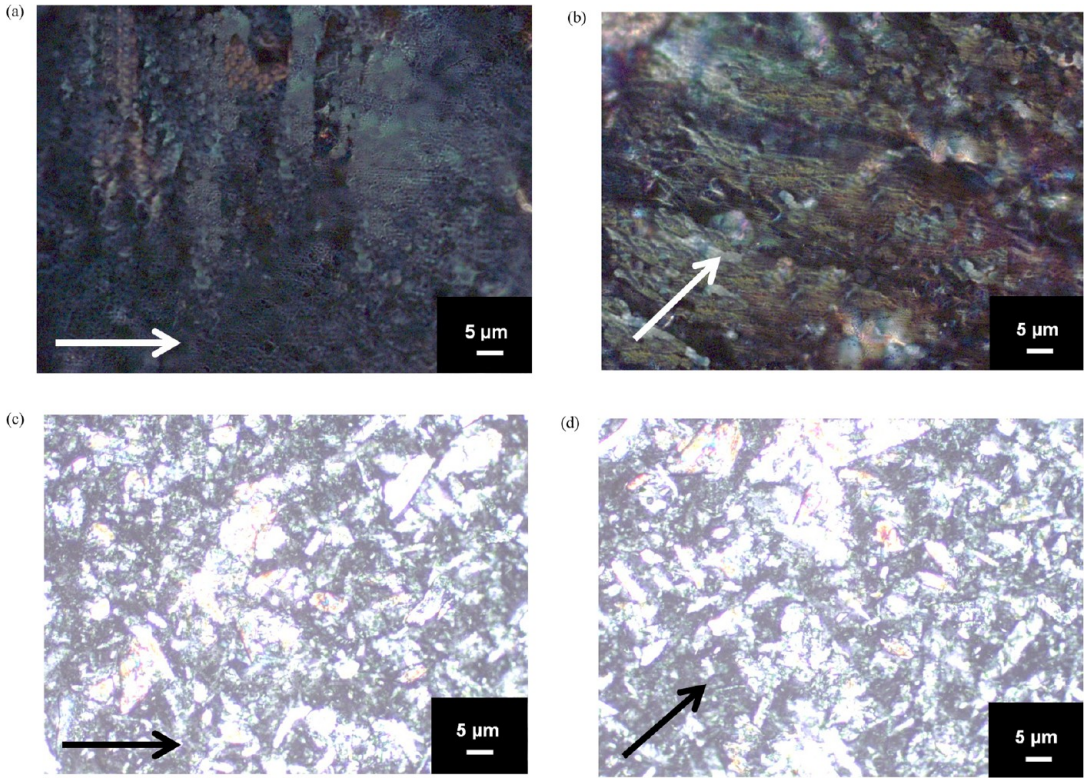

Figure 4. Polarized light microscopy images of (a) a 15 v/v % cellulose whisker reinforced all-cellulose nanocomposite produced within a magnetic field, (b) a 15 v/v % cellulose whisker reinforced all-cellulose nanocomposite produced within a magnetic field and rotated by 45° to the polarization axis, (c) a 5 v/v % cellulose whisker reinforced all-cellulose nanocomposite produced within a magnetic field, and (d) a 5 v/v % cellulose whisker reinforced all-cellulose nanocomposite produced within a magnetic field and rotated by 45° to the polarization axis. The arrows denote the direction of polarization. Images have been adjusted to +40% initial brightness to highlight domains.

dx.doi.org/10.1021/bm300746r | *Biomacromolecules* 2012, 13, 2528−2536

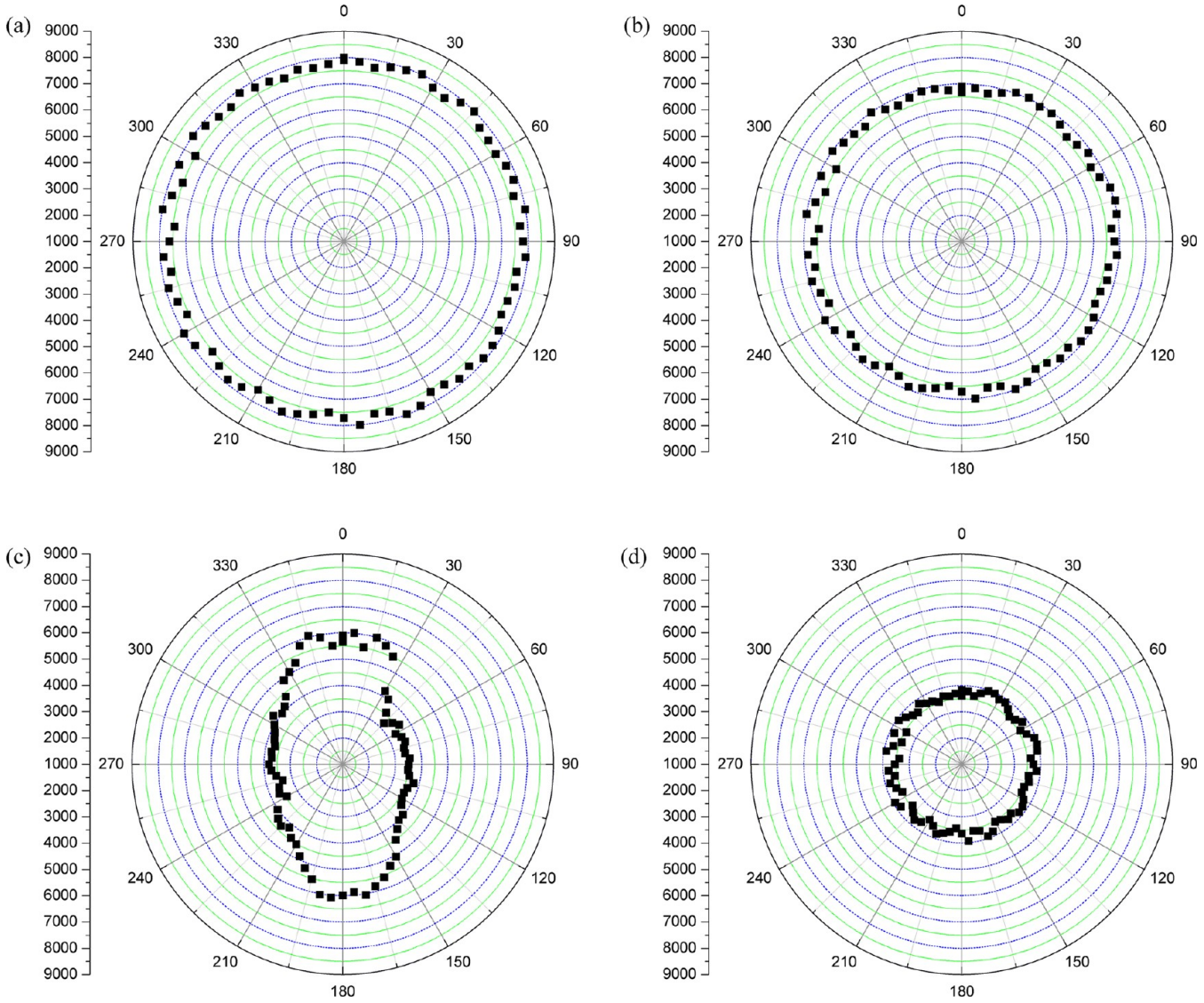

Figure 6. Intensity of the Raman band (a) located at ~1095 cm^{-1} with rotation angle for a dark domain in a 15 v/v % cellulose whisker reinforced all-cellulose nanocomposite, (b) located at ~895 cm^{-1} with rotation angle for a dark domain in a 15 v/v % cellulose whisker reinforced all-cellulose nanocomposite, (c) located at ~1095 cm^{-1} with rotation angle for a light domain in a 15 v/v % cellulose whisker reinforced all-cellulose nanocomposite, and (d) located at ~895 cm^{-1} with rotation angle for a light domain in a 15 v/v % cellulose whisker reinforced all-cellulose nanocomposite.

that both samples agree with the hypothesis that the CNWs have indeed aligned within the magnetic field.

Despite these initial indications that orientation of the CNWs occurs in the magnetic field, the increases seen are not what would be expected for a fully aligned whisker sample. The rule of mixtures can be used to predict the maximum stiffness one could expect for a fully aligned system. This rule, with the addition of an efficiency factor for the orientation of the CNWs, is described by the equation

$$E_c = \eta E_f V_f + (1 - V_f)E_m \quad (1)$$

where E_c is the modulus of the composite, E_f is the axial modulus of the nanowhiskers, E_m is the modulus of the cellulose matrix material, V_f is the volume fraction of CNWs, and η is the efficiency factor describing the orientation distribution of the reinforcing phase. For a fully aligned system, $\eta = 1$, and for a 2D in-plane random orientation distribution of CNWs, $\eta = 3/8$.[52] Eq 1 only really applies to continuous fibers, and this modulus may of course be reduced somewhat due to low aspect ratios of the CNWs. Kelly and Tyson introduce an additional parameter (η_L) into eq 1 that takes into account fibers of low aspect ratio and, therefore, low stress transfer efficiency.[53] Eq 1 then becomes

$$E_c = \eta\eta_L E_f + (1 - V_f)E_m \quad (2)$$

where η_L can vary between 0 and 1. For high aspect ratio fibers (>100), η_L is equal to 1. Typically, cellulose nanowhiskers have aspect ratios smaller than 100, although they do form percolated networks and so continuous reinforcement can be assumed.

For the transverse modulus E_T (equivalent to a sample deformed parallel to the magnetic field), the modulus prediction is given by the equation

$$E_T = \frac{E_{ft}E_m}{V_f E_m + V_m E_{ft}} \quad (3)$$

dx.doi.org/10.1021/bm300746r | Biomacromolecules 2012, 13, 2528−2536

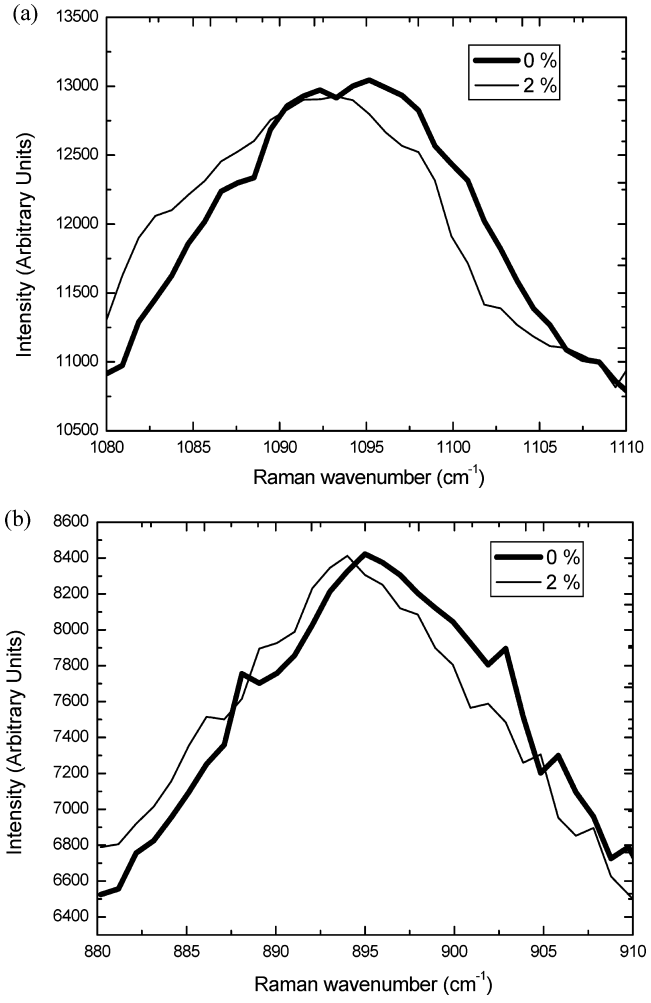

Figure 7. (a) Typical shift in the position of the Raman band located at ~1095 cm^{-1} (containing 15 v/v % of CNWs); (b) typical shift in the position of the Raman band located at ~895 cm^{-1} (containing 15 v/v % of CNWs).

where the matrix volume fraction is $V_m = 1 - V_f$ and E_{ft} is the transverse modulus of CNWs. Using a value of 143 GPa for E_f, according to Sturcova et al.,[21] E_m = 3.0 GPa and a volume fraction V_f of 0.15 gives a maximum theoretical stiffness of the composite, when the CNWs are fully aligned ($\eta = 1$) of 24 GPa. This value is almost twice that observed for the aligned sample, suggesting that optimal alignment has not occurred. A sample with randomly aligned CNWs (equivalent to the sample produced outside the magnetic field) should have, by the same calculation (but with $\eta = 3/8$), a modulus of ~11 GPa, which is very close to what is obtained for an unoriented sample (see Supporting Information). The fact that values for the composites are similar to the prediction using eq 3 suggests that the fiber length efficiency factor $\eta_L \approx 1$, approximating continuous reinforcement. This also further supports a hypothesis that incomplete orientation of the whiskers has occurred in the sample produced in the magnetic field. In the case of oriented nanowhiskers, percolation also may not occur, and so the approximation of continuous reinforcement may not apply. A prediction of $\eta_L = 0.45$ can be made in this case, using E_c = 12.5 GPa (see Supporting Information). This value is not untypical for low aspect ratio fibers, but we note that the dimensions of the CNWs used here have a large heterogeneity; values of aspect ratio are 72.8 ± 40.8. Therefore, a significant fraction of CNWs will exceed the critical value of aspect ratio of 100; misalignment of the whiskers is therefore likely to play a more dominant role than low aspect ratio.

The theoretical transverse modulus of a composite is found using eq 2. Lahiji et al.[51] report values for E_{ft} in the range 18–50 GPa (for the transverse modulus of a whisker). Using the upper and lower values of this range, and eq 2, gives values of ~3 GPa (being fairly insensitive to the value of E_{ft}) for E_T, which is much lower than the measured value, suggesting that some whiskers remain oriented in the transverse direction, despite the presence of the magnetic field. Again, the fiber length efficiency factor may also play a role here in reducing the effective stress transfer in the composite.

It was thought that perhaps a lower volume fraction of whiskers might give more "freedom" for rotation within the magnetic field. To test this hypothesis, samples with 5 v/v % of CNWs were also produced under the same conditions. Stress–strain curves for these samples are shown in Figure 3, and their mechanical properties are reported in Supporting Information. The same trends, seen for the 15 v/v % sample, are observed for this material; samples produced in the magnetic field, when deformed perpendicular to the field direction, yield enhanced stiffness and strength. The relative increase in mechanical properties is however much greater, compared to the sample produced using a 15 v/v % volume fraction of CNWs (30 and 23% increases in Young's modulus and stress at break compared to 12 and 7% for the 15 v/v % sample; these percentage increases are relative to a sample produced without the presence of the magnetic field). The modulus of the sample deformed parallel to the magnetic field direction is indeed closer to the theoretical value of the transverse modulus of the composite (~3 GPa with V_f = 0.05), suggesting that fewer CNWs are left oriented parallel to this tension axis. It is noted therefore that the volume fraction of CNWs may be an important consideration when optimizing mechanical property improvements in oriented all-cellulose nanocomposites. It is also noted that the strength of the magnetic field is not particularly high (only 1.2 T). Other published work[10−12] has used field strengths of up to 7 T to align cellulose nanofibers. Increases of ~20% (from ~4 to ~5 GPa) in storage modulus of CNWs reinforced composites have been reported.[54] The percentage increase in modulus for our samples with a lower volume fraction is close to this value.

Further evidence of alignment of the cellulose CNWs in the composites produced in the magnetic field was obtained by viewing the samples using polarized light microscopy. Optical micrographs of the samples are shown in Figure 4. In Figure 4a a polarized light image of an all-cellulose composite containing 15 v/v % of CNWs is presented. The same sample, rotated by 45° with respect to the polarization axis, is shown in Figure 4b. Light and dark domains are observed, suggesting the presence of local anisotropy. It was found that when the samples were rotated, the dark regions remained dark, whereas the lighter domains in the sample became dark, typical of local birefringence due to anisotropic orientation of domains. This type of effect has been previously reported for pressed poly(vinyl acetate)−CNWs nanocomposites; the light regions of the sample were shown to comprise oriented domains of CNWs, whereas the dark domains contained randomly oriented CNWs.[7] Figure 4c,d, for a nanocomposite produced using 5 v/v % of CNWs, show greater contrast between the light and dark domains, supporting the hypothesis that a greater degree of

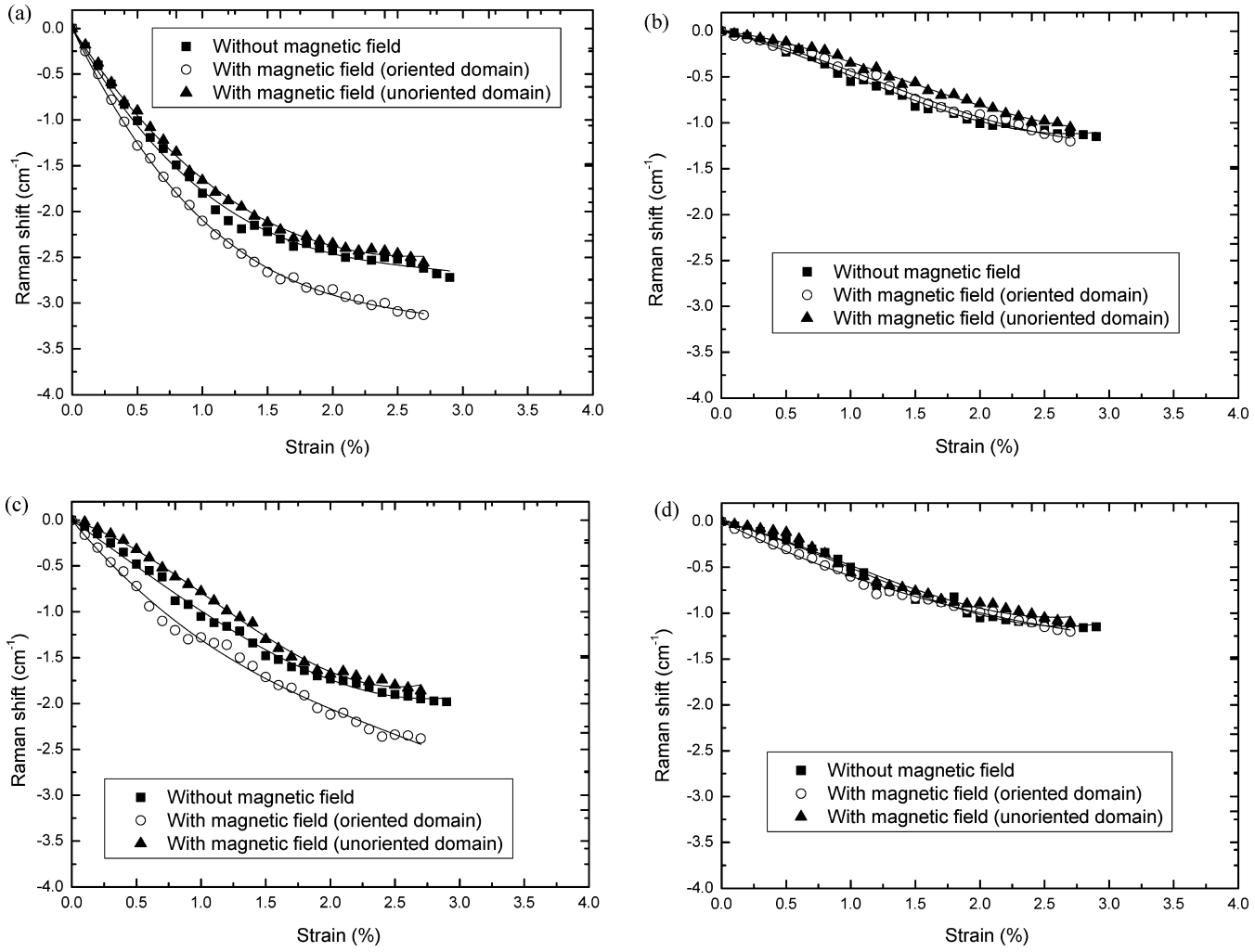

Figure 8. Shifts in the position of Raman bands located at (a) ∼1095 cm^{-1} for a 15 v/v % cellulose whisker all-cellulose nanocomposite, (b) ∼895 cm^{-1} for a 15 v/v % cellulose whisker all-cellulose nanocomposite, (c) ∼1095 cm^{-1} for a 5 v/v % cellulose whisker all-cellulose nanocomposite and (d) ∼895 cm^{-1} for a 5 v/v % cellulose whisker all-cellulose nanocomposite. Solid lines are third order polynomial fits to the data. All R^2 values for fits are >0.9.

Table 1. Mean Initial Gradients of Third Order Polynomial Fits to the Shifts in the Peak Positions of the Raman Bands Located at 1095 and 895 cm^{-1} as a Function of Strain (Data are Shown in Figure 6) for CNWs Containing All-Cellulose Nanocomposites (15 and 5 v/v % Volume Fractions)[a]

sample	1095 cm^{-1}; gradients to fit (cm^{-1} %$^{-1}$)	895 cm^{-1}; gradients to fit (cm^{-1} %$^{-1}$)
without magnetic field 15 v/v % CNWs	−1.9 (0.04)	−0.5 (0.08)
with magnetic field (oriented domain) 15 v/v % CNWs	−2.1 (0.04)	−0.5 (0.06)
with magnetic field (unoriented domain) 15 v/v % CNWs	−1.8 (0.07)	−0.4 (0.05)
without magnetic field 5 v/v % CNWs	−0.8 (0.05)	−0.5 (0.06)
with magnetic field (oriented domain) 5 v/v % CNWs	−1.2 (0.04)	−0.5 (0.05)
with magnetic field (unoriented domain) 5 v/v % CNWs	−0.8 (0.03)	−0.5 (0.04)

[a]Errors in brackets when <0.1.

orientation has occurred in this sample with the application of the magnetic field.

Light and dark regions of the samples were further analyzed using polarized Raman spectroscopy. The samples were rotated under the microscope of the spectrometer and the intensities of the bands located at ∼1095 and ∼895 cm^{-1} were recorded as function of rotation angle, in each of the domains. A typical Raman spectrum obtained from an all-cellulose nanocomposite is shown in Figure 5, with the positions of the two bands located ∼1095 cm^{-1} and ∼895 cm^{-1} highlighted. The Raman band located at ∼1095 cm^{-1} has been previously reported to correspond to the C−O stretch mode along the cellulose backbone.[55] The band located at ∼895 cm^{-1} is not present for a sample of pure CNWs, and only becomes prominent when cellulose is regenerated in the matrix phase; this band has been reported to correspond to the angle bending coordinates involving heavy atoms (e.g., CCC, COC, OCC).[56] Data from this analysis for these two bands, recorded from a dark domain are reported in Figure 6. These data show that no change in the intensity of either band occurs, indicating that both the nanowhiskers and matrix phase exhibit no preferred orientation in these domains (Figure 6a and b, respectively). In the light regions, however, pronounced anisotropy and orientation of the CNWs is observed, with a large change in the intensity of the band located at ∼1095 cm^{-1} with rotation angle (Figure 6c).

dx.doi.org/10.1021/bm300746r | Biomacromolecules 2012, 13, 2528−2536

No change in the intensity of the band located at ~895 cm^{-1} occurs (Figure 6d), suggesting that the matrix phase remains unoriented, even with the application of the magnetic field. Similar data are obtained for the 5 v/v % samples (see Supporting Information).

To assess the effect of the orientation of the nanowhiskers on stress-transfer within the all-cellulose composites, the positions of the Raman bands located at ~1095 and ~895 cm^{-1} were monitored during tensile deformation. Both these bands are found to shift in position when the samples are deformed (Figure 7a,b), which indicates that stress transfers through the materials leading to direct molecular deformation of the cellulose molecular chains. As already stated, the Raman bands located at ~1095 and ~895 cm^{-1} are thought to correspond to the reinforcing phase (CNWs or cellulose Iβ) and the matrix (regenerated cellulose II), respectively, although the former is a mixed mode vibration arising from both components.[32] Detailed shifts in these peak positions are reported in Figure 8 for both light (oriented) and dark (unoriented) domains in the samples. It is clear that both bands shift, in a nonlinear manner, toward a lower wavenumber position upon deformation. The data were fitted using a third order polynomial function, which was subsequently differentiated to obtain the initial gradient of the shifts (reported in Table 1). The profiles of the shifts in the position of the Raman band located at ~1095 cm^{-1} with respect to strain reflect the shape of the stress−strain curves shown in Figures 2 and 3. It is also noted that the values of the initial gradients of the shifts are higher for the Raman band located at ~1095 cm^{-1} than for the band located at ~895 cm^{-1} (see Table 1). Both of these observations point to the fact that the mechanical properties of the nanocomposites appear to be largely dictated by the CNWs and not the matrix; some stress transfer occurs within the matrix itself but mostly transfers to the stiffer phase (CNWs), as is typically seen for fiber reinforced composites. The profile of the shifts in the position of the band located at ~895 cm^{-1} are also different to the band at ~1095 cm^{-1}; the gradient of the data from the band located at 895 cm^{-1} is initially relatively flat, increasing with strain, eventually reaching a plateau at high strain. This suggests that the orientation of the matrix phase may change during deformation, although we have no evidence of this effect.

The gradient of the shift for the Raman band located at ~1095 cm^{-1} for a light region (oriented CNWs) of a 15 v/v % all-cellulose composite (Figure 8a) is much larger than that seen for a dark region (unoriented CNWs). In fact, the gradient of the data obtained from the latter is similar to that obtained from a sample cured without the presence of a magnetic field. This difference clearly shows the effect of orientation on the enhancement of stiffness, and therefore shift rate with respect to strain, within oriented domains of the sample. In the matrix phase, characterized by the shift in the position of the band located at ~895 cm^{-1} (Figure 8b), little difference can be seen between both domains, and a sample produced without the presence of a magnetic field; again this points to the fact that the CNWs dictate the mechanical properties of the materials. When the volume fraction of CNWs was decreased to 5 v/v %, a much pronounced difference between the gradient of the shift in the peak located at ~1095 cm^{-1} for an oriented and an unoriented domain is noted (Figure 8c and Table 1). This is further evidence that at a lower volume fraction there is more "space" for the CNWs to orient. The matrix behavior is similar to the 15 v/v % sample (cf. Figure 8d with b).

Rod-like molecules are known to possess an excluded volume, which prevents them from passing through each other. To maximize entropy, rod-like molecules will tend toward a random distribution of orientations, maximizing translational entropy at low concentrations.[57] Translational entropy is coupled to positional entropy, and this component becomes more dominant at higher concentrations.[57] At a critical concentration of the molecules, the only way for them to continue to maximize entropy is to align and increase positional entropy because they cannot cross due to their excluded volume; this is the nematic state. The question remains, however, as to why unoriented domains remain in samples that are cured in the presence of a magnetic field? The presence of this field encourages alignment of the CNWs into an oriented state, but their tendency is toward a high entropy state, and so some randomly oriented domains remain. If lower volume fractions of CNWs are used, then there is less influence of excluded volume on this orientation effect, and they can more readily align, leading to a greater relative increase in axial stiffness of the material compared to the unoriented state. We have no detailed information on the concentration of CNWs in the oriented domains, and indeed there may be local variations in concentrations. It may be that there is a competition between the effect of nematic and magnetic field orientation and the entropic drivers toward a random state, leaving unoriented domains. If, during the curing process of the composite, the concentration of whiskers reaches a particular level, orientation may occur through a nematic process, additionally assisted by the magnetic field. Higher magnetic field strengths (in the range 5−20 T) have been used to align CNWs in suspension and in a composite. It could be, therefore, that a great deal of optimization of the properties of all-cellulose nanocomposites, and indeed nanocomposites comprising CNWs in general, could be achieved by the variation of magnetic field strength and CNWs concentration. The use of Raman spectroscopy would be a useful way to assess this optimization and effect on the mechanical interfaces present in these new and emerging materials.

CONCLUSIONS

Raman spectroscopy has been demonstrated to be a powerful tool for following the micromechanics of oriented cellulose nanowhisker reinforced all-cellulose nanocomposites. The presence of a magnetic field during the curing process of these nanocomposites has been shown to induce orientation of the nanowhiskers, but only partially. Domain structures within the composites are noted for a high volume fraction sample, and only when this is reduced is there sufficient freedom for the nanowhiskers to rotate. This effect results in a higher relative increase in the stiffness and strength of a nanocomposite produced using the lower volume fraction of the nanowhiskers. Both the molecular deformation and orientation in the nanowhisker and matrix phase of the composites has been probed. It has been shown that little orientation of the matrix occurs when the magnetic field is applied. Pronounced orientation of the nanowhiskers is noted, in some domains of the material, when the magnetic field is applied, but some domains are present where random orientation of the nanowhiskers remains. This textured property of the nanocomposites is thought to be due to a competition between maximizing entropy, by nanowhiskers remaining in random orientations, and the effect of the magnetic field. It is thought that if concentrations of nanowhiskers and the strength of the

magnetic field are further controlled then optimization of the mechanical properties could be achieved.

■ ASSOCIATED CONTENT

Supporting Information

Tables S1 and S2 giving the mechanical data and Figure S3 giving the intensity data for the 5 v/v % CNWs sample. This material is available free of charge via the Internet at http://pubs.acs.org.

■ AUTHOR INFORMATION

Corresponding Author

*E-mail: s.j.eichhorn@exeter.ac.uk. Tel.: +44(0)1392 72 5515. Fax: +44(01)1392 21 7965.

Present Address

†College of Engineering, Mathematics and Physical Sciences, University of Exeter, Physics building, Stocker Road, Exeter, EX4 4QL, U.K.

Notes

The authors declare no competing financial interest.

■ ACKNOWLEDGMENTS

We thank the Royal Thai Government for a Ph.D scholarship for T.P.

■ REFERENCES

(1) Eichhorn, S. J.; Dufresne, A.; Aranguren, M.; Marcovich, N. E.; Capadona, J. R.; Rowan, S. J.; Weder, C.; Thielemans, W.; Roman, M.; Renneckar, S.; Gindl, W.; Veigel, S.; Keckes, J.; Yano, H.; Abe, K.; Nogi, M.; Nakagaito, A. N.; Mangalam, A.; Simonsen, J.; Benight, A. S.; Bismarck, A.; Berglund, L. A.; Peijs, T. *J. Mater. Sci.* **2010**, *45*, 1−33.

(2) Eichhorn, S. J. *Soft Matter* **2011**, *7*, 303−315.

(3) Klemm, D.; Kramer, F.; Moritz, S.; Lindström, T.; Ankerfors, M.; Gray, D.; Dorris, A. *Angew. Chem., Int. Ed.* **2011**, *50*, 5438−5466.

(4) Habibi, Y.; Lucia, L. A.; Rojas, O. J. *Chem. Rev.* **2010**, *110*, 3479−3500.

(5) Siro, I.; Plackett, D. *Cellulose* **2010**, *17*, 459−494.

(6) Revol, J. F.; Bradford, H.; Giasson, J.; Marchessault, R. H.; Gray, D. G. *Int. J. Biol. Macromol.* **1992**, *14*, 170−172.

(7) Rusli, R.; Shanmuganathan, K.; Rowan, S. J.; Weder, C.; Eichhorn, S. J. *Biomacromolecules* **2010**, *11*, 762−768.

(8) Herrera, N. V.; Mathew, A. P.; Wang, L. Y.; Oksman, K. *Plast., Rubber Compos.* **2011**, *40*, 57−64.

(9) Iwamoto, S.; Isogai, A.; Iwata, T. *Biomacromolecules* **2011**, *12*, 831−836.

(10) Revol, J. F.; Godbout, L.; Dong, X. M.; Gray, D. G.; Chanzy, H.; Maret, G. *Liq. Cryst.* **1994**, *16*, 127−134.

(11) Sugiyama, J.; Chanzy, H.; Maret, G. *Macromolecules* **1992**, *25*, 4232−4234.

(12) Kvien, I.; Oksman, K. *Appl. Phys. A: Mater. Sci. Process.* **2007**, *87*, 641−643.

(13) Bordel, D.; Putaux, J. L.; Heux, L. *Langmuir* **2006**, *22*, 4899−4901.

(14) Csoka, L.; Hoeger, I. C.; Peralta, P.; Peszlen, I.; Rojas, O. J. *J. Colloid Interface Sci.* **2011**, *363*, 206−212.

(15) Gindl, W.; Emsenhuber, G.; Maier, G.; Keckes, J. *Biomacromolecules* **2009**, *10*, 1315−1318.

(16) Tatsumi, M.; Teramoto, Y.; Nishio, Y. *Biomacromolecules* **2012**, *13*, 1584−1591.

(17) Sakurada, I.; Nukushina, Y.; Ito, T. *J. Polym. Sci.* **1962**, *57*, 651.

(18) Cintron, M. S.; Johnson, G. P.; French, A. D. *Cellulose* **2011**, *18*, 505−516.

(19) Eichhorn, S. J.; Davies, G. R. *Cellulose* **2006**, *13*, 291−307.

(20) Iwamoto, S.; Kai, W. H.; Isogai, A.; Iwata, T. *Biomacromolecules* **2009**, *10*, 2571−2576.

(21) Sturcova, A.; Davies, G. R.; Eichhorn, S. J. *Biomacromolecules* **2005**, *6*, 1055−1061.

(22) Huber, T.; Mussig, J.; Curnow, O.; Pang, S. S.; Bickerton, S.; Staiger, M. P. *J. Mater. Sci.* **2012**, *47*, 1171−1186.

(23) Nishino, T.; Matsuda, I.; Hirao, K. *Macromolecules* **2004**, *37*, 7683−7687.

(24) Qin, C.; Soykeabkaew, N.; Xiuyuan, N.; Peijs, T. *Carbohydr. Polym.* **2008**, *71*, 458−467.

(25) Soykeabkaew, N.; Arimoto, N.; Nishino, T.; Peijs, T. *Compos. Sci. Technol.* **2008**, *68*, 2201−2207.

(26) Soykeabkaew, N.; Sian, C.; Gea, S.; Nishino, T.; Peijs, T. *Cellulose* **2009**, *16*, 435−444.

(27) Arevalo, R.; Picot, O. T.; Wilson, R. M.; Soykeabkaew, N.; Peijs, T. *J. Biobased Mater. Bioenergy* **2010**, *4*, 129−138.

(28) Duchemin, B. J. C.; Mathew, A. P.; Oksman, K. *Composites, Part A* **2009**, *40*, 2031−2037.

(29) Duchemin, B. J. C.; Newman, R. H.; Staiger, M. P. *Compos. Sci. Technol.* **2009**, *69*, 1225−1230.

(30) Gindl, W.; Keckes, J. *Polymer* **2005**, *46*, 10221−10225.

(31) Gindl, W.; Martinschitz, K. J.; Boesecke, P.; Keckes. *Compos. Sci. Technol.* **2006**, *66*, 2639−2647.

(32) Pullawan, T.; Wilkinson, A. N.; Eichhorn, S. J. *Compos. Sci. Technol.* **2010**, *70*, 2325−2330.

(33) Hamad, W. Y.; Eichhorn, S. *ASME J. Eng. Mater. Technol.* **1997**, *119*, 309−313.

(34) Eichhorn, S. J.; Hughes, M.; Snell, R.; Mott, L. *J. Mater. Sci. Lett.* **2000**, *19*, 721−723.

(35) Eichhorn, S. J.; Young, R. J. *Cellulose* **2001**, *8*, 197−207.

(36) Peetla, P.; Schenzel, K. C.; Diepenbrock, W. *Appl. Spectrosc.* **2006**, *60*, 682−691.

(37) Gierlinger, N.; Schwanninger, M.; Reinecke, A.; Burgert, I. *Biomacromolecules* **2006**, *7*, 2077−2081.

(38) Eichhorn, S. J.; Young, R. J. *Compos. Sci. Technol.* **2004**, *64*, 767−772.

(39) Bulota, M.; Tanpichai, S.; Hughes, M.; Eichhorn, S. J. *ACS Appl. Mater. Interfaces* **2012**, *4*, 331−337.

(40) Rusli, R.; Shanmuganathan, K.; Rowan, S. J.; Weder, C.; Eichhorn, S. J. *Biomacromolecules* **2011**, *12*, 1363−1369.

(41) Rusli, R.; Eichhorn, S. J. *Nanotechnology* **2011**, *22*, 325706.

(42) Mendez, J.; Annamalai, P. K.; Eichhorn, S. J.; Rusli, R.; Rowan, S. J.; Foster, E. J.; Weder, C. *Macromolecules* **2011**, *44*, 6827−6835.

(43) Bakri, B.; Eichhorn, S. J. *Cellulose* **2010**, *17*, 1−11.

(44) van den Berg, O.; Capadona, J. R.; Weder, C. *Biomacromolecules* **2007**, *8*, 1353−1357.

(45) Yuan, H.; Nishiyama, Y.; Wada, M.; Kuga, S. *Biomacromolecules* **2006**, *7*, 696−700.

(46) Elazzouzi-Hafraoui, S.; Nishiyama, Y.; Putaux, J.-L.; Heux, L.; Dubreuil, F.; Rochas, C. *Biomacromolecules* **2007**, *9*, 57−65.

(47) Marquardt, D. W. *J. Soc. Ind. Appl. Math.* **1963**, *11*, 431−441.

(48) Gindl, W.; Martinschitz, K. J.; Boesecke, P.; Keckes, J. *Biomacromolecules* **2006**, *7*, 3146−3150.

(49) Gindl, W.; Keckes, J. *J. Appl. Polym. Sci.* **2007**, *103*, 2703−2708.

(50) Nishino, T.; Arimoto, N. *Biomacromolecules* **2007**, *8*, 2712−2716.

(51) Lahiji, R. R.; Xu, X.; Reifenberger, R.; Raman, A.; Rudie, A.; Moon, R. J. *Langmuir* **2010**, *26*, 4480−4488.

(52) Krenchel, H., *Fibre Reinforcement*; Academisk Forlag: Copenhagen, 1964.

(53) Kelly, A.; Tyson, W. R. *J. Mech. Phys. Solids* **1965**, *13*, 329−350.

(54) Li, D.; Liu, Z.; Al-Haik, M.; Tehrani, M.; Murray, F.; Tannenbaum, R.; Garmestani, H. *Polym. Bull.* **2010**, *65*, 635−642.

(55) Wiley, J. H.; Atalla, R. H. *Carbohydr. Res.* **1987**, *160*, 113−129.

(56) Atalla, R. H.; Nagel, S. C. *Science* **1974**, *185*, 522−523.

(57) Onsager, L. *Ann. N. Y. Acad. Sci.* **1949**, *51*, 627−659.